An investigation of surface contamination introduced during He^+ implantation and subsequent effects on the thermal oxidation of Cu

Subing Yang, Yuki Nakagawa, Tamaki Shibayama*

Faculty of Engineering, Hokkaido University, Sapporo, Hokkaido 060-8628, Japan

* Corresponding author.
E-mail address: shiba@qe.eng.hokudai.ac.jp

Abstract

Ion implantation is a potential means of increasing the oxidation resistance of Cu. However, carbonaceous contamination can also be introduced onto the metal surface during this process as a consequence of pump oil within the vacuum system. This can complicate analysis of the effect of ion implantation on Cu oxidation. The present study examined the surface contamination introduced during He^+ implantation. Carbonaceous contamination was indeed identified on the Cu surface and had an obvious passivation effect on Cu oxidation at 200 °C. This was ascribed to the implantation of C into the Cu to a depth of several nanometers in conjunction with He^+ implantation. The Cu was protected from oxidation by the formation of a layer consisting of C, Cu and a small amount of Cu_2O that inhibited the inward diffusion of oxygen.

Key words: copper; oxidation; implantation; microstructure.

1. Introduction

Owing to its excellent thermal and electrical conductivities, mechanical workability, overall non-toxicity and good availability, copper (Cu) is widely used in numerous applications, such as in piping, electrical systems and electronic devices [1,2]. However, Cu readily undergoes native oxidation even at room temperature [3], and the oxidation and corrosion of Cu used in certain industrial applications after several working cycles can degrade its performance [2,4] and also limit the potential technological applications of this metal. As an example, Cu is a potential replacement for the tin-lead solder alloys currently found in electronic packaging, but the issue of oxidation must first be addressed [2,5]. Various technologies have been proposed to increase the oxidation resistance of Cu, such as surface passivation with organic compounds, inorganic materials or carbon-based substances serving as oxidation inhibitors. However, their large-scale application has had limited success [1,6]. Furthermore, with the increasing concern about environmental pollution and human health, some potential organic inhibitors are no longer of interest because of their high toxicity [7]. Furthermore, many common anti-oxidation techniques, such as alloying and electroplating, can degrade certain physical properties, such as thermal and electrical conductivities [1]. Thus, there is an urgent need to develop techniques to increase the oxidation resistance of Cu while avoiding significant loss of thermal and electrical properties.

The selective incorporation of alloying elements via ion implantation has been explored as a possible means of improving surface oxidation resistance.

This technique allows any element to be introduced into the near-surface region of a solid in a controlled and reproducible manner [8], and it is independent of most equilibrium constraints [9]. Qin et al. [10] determined that the corrosion resistance of Ni-Al bronzes was improved following surface modification by Cr^+ implantation. Additionally, Zhao et al. [11] has reported that the implantation of Cr, Al and Mg to shallow depths of approximately 100 nm enhances the oxidation resistance of Cu films having thicknesses of approximately 800 nm but does not significantly affect their conductivity. These effects occur because the implanted ions are concentrated at the film surface. Thus, ion implantation may prevent the oxidation of Cu and allow the application of this metal in various electronic applications and ultra-large-scale integration [2,11].

Interestingly, the metal surface is often contaminated during ion implantation, which is widely believed to be attributed to the pump oil within vacuum system [12,13]. This carbonaceous contamination is thought to provide additional protection from oxidation. However, to date, the mechanism by which this coating prevents Cu oxidation has been poorly understood. In particular, few reports have investigated the microstructures associated with Cu oxidation when this contamination is present. Obviously, this carbonaceous contamination effect complicates the analysis of the passivation imparted by implanting ions such as Cr^+ or Al^+. Therefore, it is important to clearly understand the effect of a carbonaceous coating introduced onto the metal surface during ion implantation on Cu oxidation. Furthermore, both oxidation and corrosion are fundamental problems

associated with other widely used metals, and ion implantation has also been extensively investigated with regard to increasing the oxidation and corrosion resistance of substances, such as metallic biomaterials [14] and magnesium alloys [10, 15], in recent years. As an example, the corrosion residence of medical-grade titanium metal and its alloys has been shown to be improved by N^+ implantation [16-18]. Thus, carbonaceous contamination may also be introduced onto the surfaces of these metals during ion implantation, although this effect is rarely considered or reported. Cu is considered a good model for the analysis of the formation of metal oxides in general. Therefore, a detailed understanding of the effect of this carbonaceous contamination introduced onto the metal surface during ion implantation on the oxidation of Cu would also be applicable to other metals. Additionally, graphene [19,20] and other carbonaceous materials (such as carbon dots [7]) have received increasing attention as surface passivation materials for Cu. Therefore, a good understanding of the effect of this carbonaceous contamination on Cu oxidation could assist in finding applications for other carbonaceous materials intended to prevent Cu oxidation.

In the present study, carbonaceous contamination was introduced during ion implantation and the consequent variations in the microstructure of the Cu during oxidation were investigated. To avoid the alloying effect and damage that result from the ion implantation process, inert He^+ ions were used. The oxidation of Cu with and without He^+ implantation was analyzed by employing various microscopy techniques. The data confirm that

carbonaceous contamination was deposited on the Cu surface during ion implantation, resulting in an obvious passivation effect on Cu oxidation. Observations using transmission electron microscopy (TEM) established that a layer structure comprising C, Cu and a small amount of Cu_2O was formed on the surface of the Cu after He^+ implantation and protected the Cu from the oxidation by hindering oxygen diffusion into the metal.

2. Experimental

2.1. Materials and ion implantation

Bulk specimens of polycrystalline Cu (99.99%, 10×10×1 mm) were purchased from the Nilaco Corporation (Tokyo, Japan, part no. 1054). The surface of this bulk Cu was degreased by polishing with #1500 emery paper followed by mechanical polishing to a mirror finish using a buff grinder with 0.1 CR alumina as the polishing agent. Each sample was subsequently mechanically polished for 10 min using a buff grinder with deionized water to remove any residual alumina. Following this, each specimen was cleaned ultrasonically in acetone and in deionized water sequentially twice, rinsed with deionized water, and dried in air.

The 100 keV He^+ implantation trials were performed at room temperature on a Cu substrate with an injection angle of 90° and a fluence of 5.0×10^{15} cm^{-2} with an ion flux of 6.2×10^{12} cm^{-2} s^{-1}. Raster scanning of the ion beam was applied to ensure homogeneous irradiation and a vacuum of at least 1.0×10^{-5} Pa was achieved prior to implantation. The He^+ ion penetration profile was calculated using the SRIM 2013 software [21] using the full

damage cascade model with the assumption of a sample density of 8.96 $g \cdot cm^{-3}$ [22] and a Cu threshold displacement energy of 25 eV. The total penetration depth predicted by the calculation was approximately 620 nm with maximum doping in the vicinity of 330 nm.

After ion implantation, in the case of some samples, the area over which He^+ ions had been implanted was cleaned using acetone and deionized water to remove any carbonaceous contamination absorbed on the Cu surface. This cleaning process was repeated until the analysis of the surface composition using scanning electron microscopy with energy dispersive X-ray spectroscopy (SEM-EDS) did not show any obvious change between subsequent cleanings. Three types of Cu samples were prepared: pristine Cu, He^+-implanted Cu and He^+-implanted Cu with subsequent surface cleaning (referred to herein as He^+-implanted + cleaned Cu).

2.2. Oxidation experiments

To allow detailed observations of the evolution of Cu oxidation, a slow oxidation rate was obtained by heating the samples at a relatively low temperature of 200 ºC. The samples prepared as in Section 2.1 were heated at 200 ºC for 30 min, 1 h or 3 h in ambient air using a tube furnace (KDF-S70), after which each specimen was cooled in air. During these trials, the furnace was equilibrated at the target temperature for 30 min before the sample was transferred into the tube.

2.3 Characterization

Images of the Cu surfaces were acquired using a Nikon Eclipse LV150 optical microscope. Raman spectra were obtained with a Raman microscope

(HORIBA XploRA) equipped with a 532 nm laser and a 2400 groove/nm grating, employing confocal Raman microscopy with a confocal aperture of 100 μm. X-ray photoelectron spectroscopy (XPS) analyses (JEOL JPS-9200) were performed with a standard Al Kα X-ray source, using a measurement area 1.0 mm in diameter at a pressure of 10^{-7} Pa. A Shirley background subtraction was performed prior to curve fitting and all spectral positions were corrected by normalizing the data relative to the intensity of the C 1s peak at 284.8 eV. Owing to the shallow oxidation layers obtained in this study, variations in oxidation products in the depth direction were examined using an XPS etching technique. The etching was carried out with a 2 keV Ar^+ ion beam with an etching size of 3×3 mm and etching rate of approximately 2 nm/min.

The surface morphologies of samples were examined by field emission scanning electron microscopy (FE-SEM; JEOL JSM–7001FA) at an accelerating voltage of 15 kV. The TEM samples were prepared using gallium ions with a focused ion beam (FIB) system (JEOL, JEM-90320FIB). The ion accelerating voltage was 30 kV and the samples were thinned to a final thickness of approximately 100 nm. To protect the sample surfaces from being damaged by the FIB, each specimen was precoated with carbon using the finest beam (Beam 9 setting on the JEM-90320FIB). This process gave a carbon thickness of approximately 1 μm. Potential damage to the TEM samples that resulted from the gallium ions during the FIB treatment was removed by subsequent polishing with lower energy Ar^+ ions using a GentleMill system (Technoorg Linda Co., Ltd., Gentle Mill IV8 HI). Both

sides of each TEM sample were polished with a 1.5 kV beam at an 15º angle of incidence for 2 min, followed by a 0.3 kV beam at 10º for 20 min. Microstructural observations were performed with a JEOL JEM-2000FX at 200 kV. High-resolution TEM (HR-TEM) and high-angle annular dark field (HAADF) scanning transmission electron microscopy (STEM) analyses were performed using a Cs-corrected STEM (FEI, Titan G2 60-300) operating at 300 kV.

3. Results

3.1 Cu morphology variations after He^+ implantation

After implantation, neither optical images (which examined color variations) nor SEM images (which assessed morphology) indicated major variations (Figs. 1(a) to 1(d)). However, a slight change in color after treatment seems apparent in Fig. 1(b). This effect may have resulted from the formation of Cu_2O, as is also indicated by the Raman spectrum of the material (Fig. 1(e)). Nevertheless, the intensity of the Cu_2O Raman peak was relatively weak, suggesting that the amount of Cu_2O in the specimen was minimal. The cross-sectional TEM image in Fig. 1(f) shows no distinct defects induced by He^+ implantation, as a consequence of the relatively low implantation fluence that was applied. A cross-section TEM image of a He^+-implanted Cu sample exposed to a fluence of 5.0×10^{16} cm^{-2} is provided in Fig. S1 for comparison. This material clearly shows implantation-induced defects, the distribution of which is in good agreement with the results of calculations using the SRIM software.

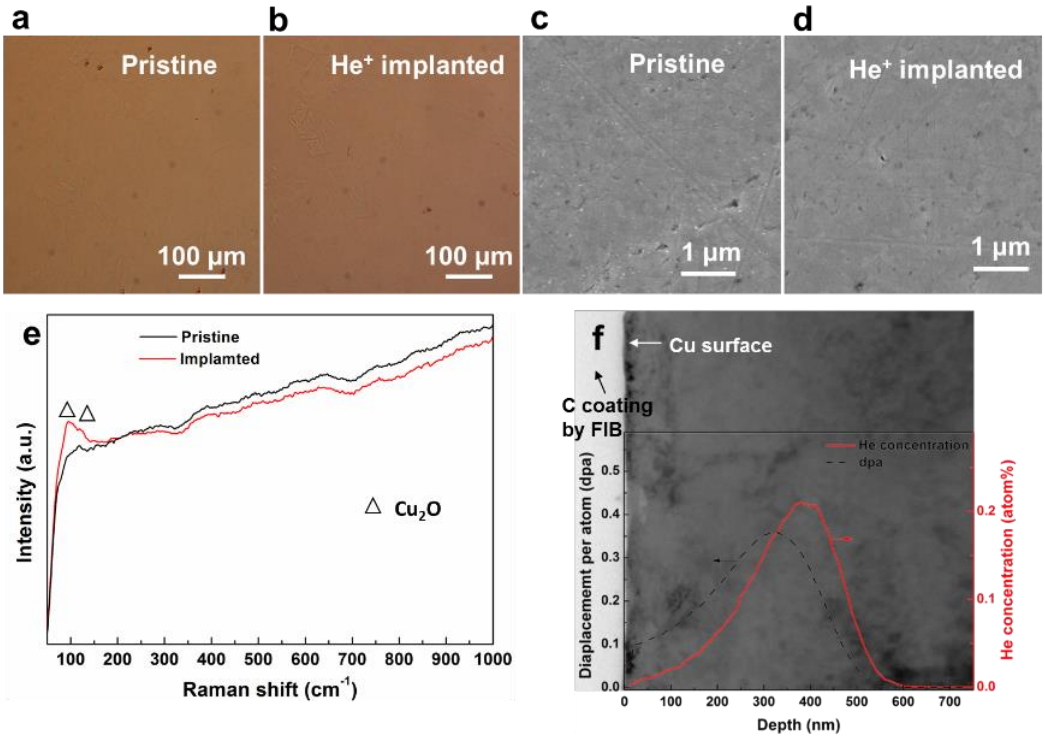

Fig. 1. (a, b) Optical and (c, d) SEM images showing the surface morphology of (a, c) pristine Cu and (b, d) He^+-implanted Cu. (e) Raman spectra of pristine and He^+-implanted Cu. (f) A cross-sectional TEM image of He^+-implanted Cu processed with a fluence of 5.0×10^{15} cm^{-2}.

3.2 Thermal oxidation of Cu with and without He^+ implantation

Cu specimens with and without ion implantation exhibited significant surface color variations after being heated at 200 ºC for 30 min. A reddish surface coloration was observed on the pristine Cu, while the He^+-implanted material retained essentially all of its original metallic luster (Figs. 2(a) and (b)). Raman spectra demonstrated that Cu_2O was formed on the surfaces of both samples (Fig. 2(c)). However, the peak at 218 cm^{-1}, which is typically the strongest Cu_2O peak [23], was almost undetectable in the spectrum of the

He^+-implanted Cu. This result suggests that this specimen was less oxidized than the pristine Cu [24]. The surface morphology of the pristine Cu also became uneven and bumpy after heating for 30 min (Fig. 2(d)). Cu_2O grows on a Cu surface generally via the nucleation and coalescence of oxide islands, and the nodule structure in Fig. 2(d) is therefore attributed to these islands and/or their coalescence. In contrast, the surface of the He^+-implanted Cu remained relatively smooth with few oxide islands (Fig. 2(e)), again suggesting a lesser degree of oxidation.

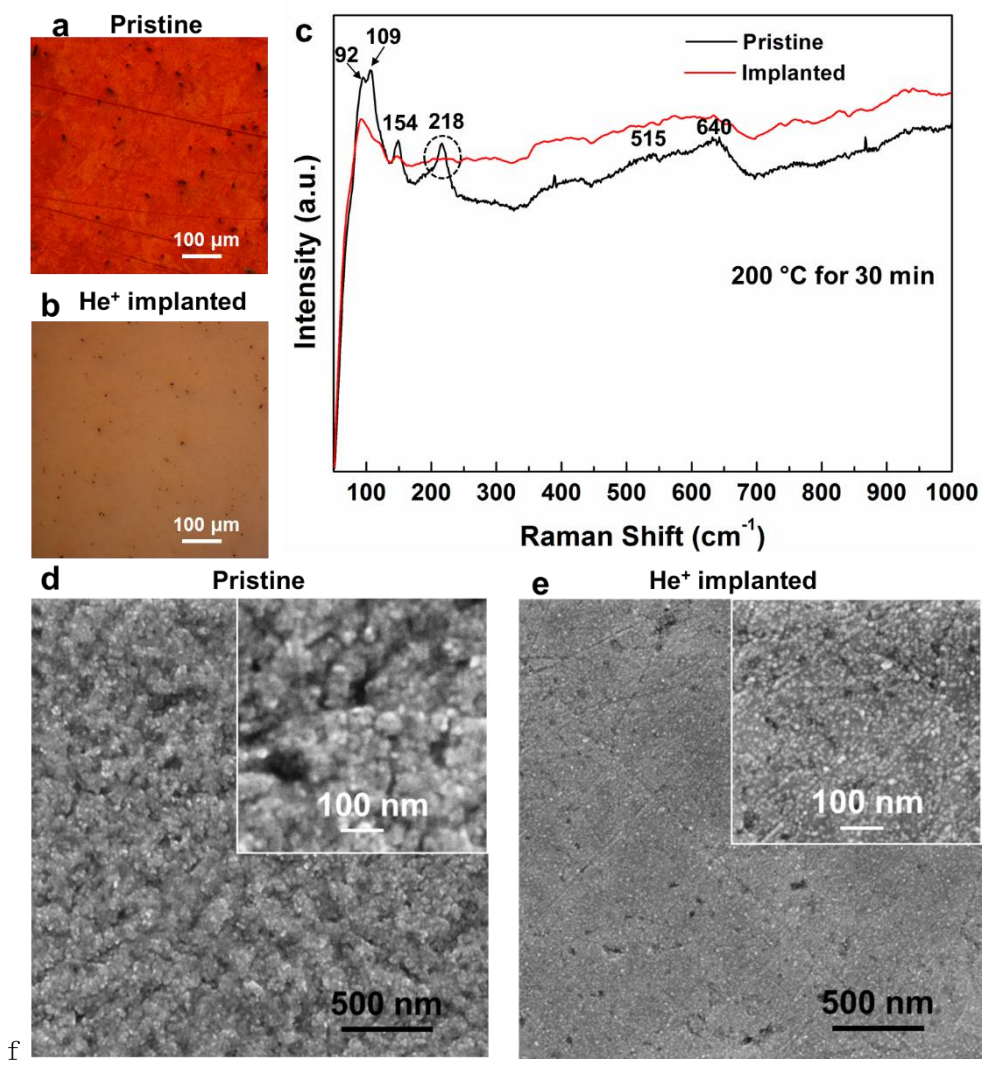

f

Fig. 2. (a, b) optical images, (c) Raman spectra and (d, e) SEM images of (a, d) pristine

Cu and (b, e) He^+-implanted Cu after heating at 200 °C for 30 min. The insets in (d and e) are SEM images obtained with higher magnification.

Upon increasing the heating time to 1 h, the surface of the He^+-implanted Cu also became red (Fig. 3(b)) while the pristine sample took on a darker red coloration (Fig. 3(a)). The Raman spectra show that Cu_2O continued to be the sole oxidation product on both samples (Fig. 3(c)). Both materials generated very similar spectra, especially in the case of the peak at 218 cm^{-1}. The surface morphologies of these two samples also became similar, in that the surface of the He^+-implanted Cu was uneven and showed a nodular structure (Figs. 3(d) and 3(e)).

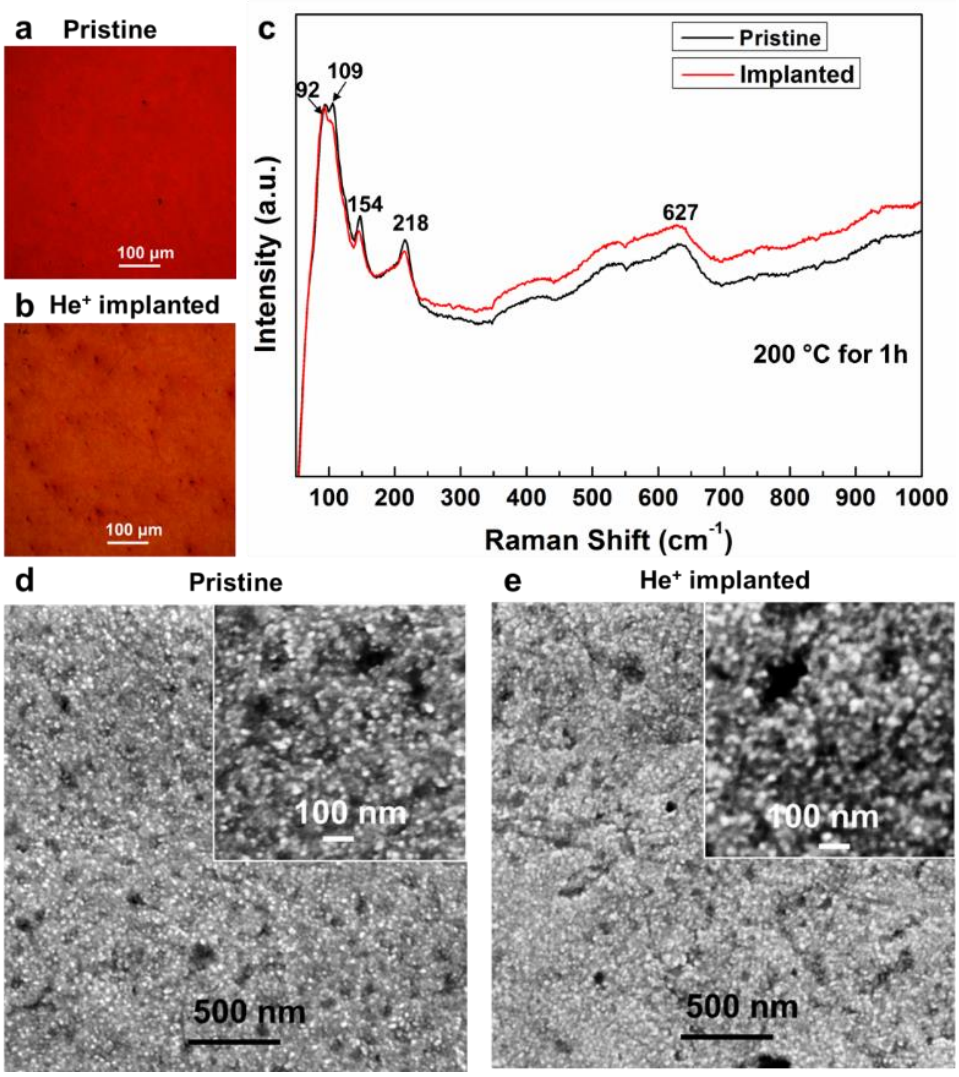

Fig. 3. (a, b) Optical images, (c, d) SEM images, and (e) Raman spectra of (a, c) pristine Cu and (b, d) He^+-implanted Cu after heating at 200 °C for 1 h. The insets in (c and d) are SEM images acquired with higher magnification.

After heating at 200 °C for 3 h, a gray coloration appeared on the pristine Cu (Fig. 4(a)) that was identified as CuO by Raman microscopy (Fig. 4(c)). The surface of the He^+-implanted Cu took on a more obvious red coloration (Fig. 4(b)) and the sole oxidation product was still Cu_2O (Fig. 4(c)). The surface morphology of the He^+-implanted Cu after heating for 3 h (Fig. 4(e))

was similar to that after heating for 1 h (Fig. 3(e)) except that it was more uneven and had larger oxide particles. The surface of the pristine Cu became somewhat more planar but with more oxide particles (Fig. 4(d)). These oxide particles were too numerous to allow the substrate to be viewed from overhead in the SEM images, and so a tilted view of the surface is provided as an inset image to Fig. 4(d). The changes in the surface color, morphology and Raman spectra of these samples after heating indicate that the oxidation of the He^+-implanted sample during heating at 200 °C was inhibited up to 3 h.

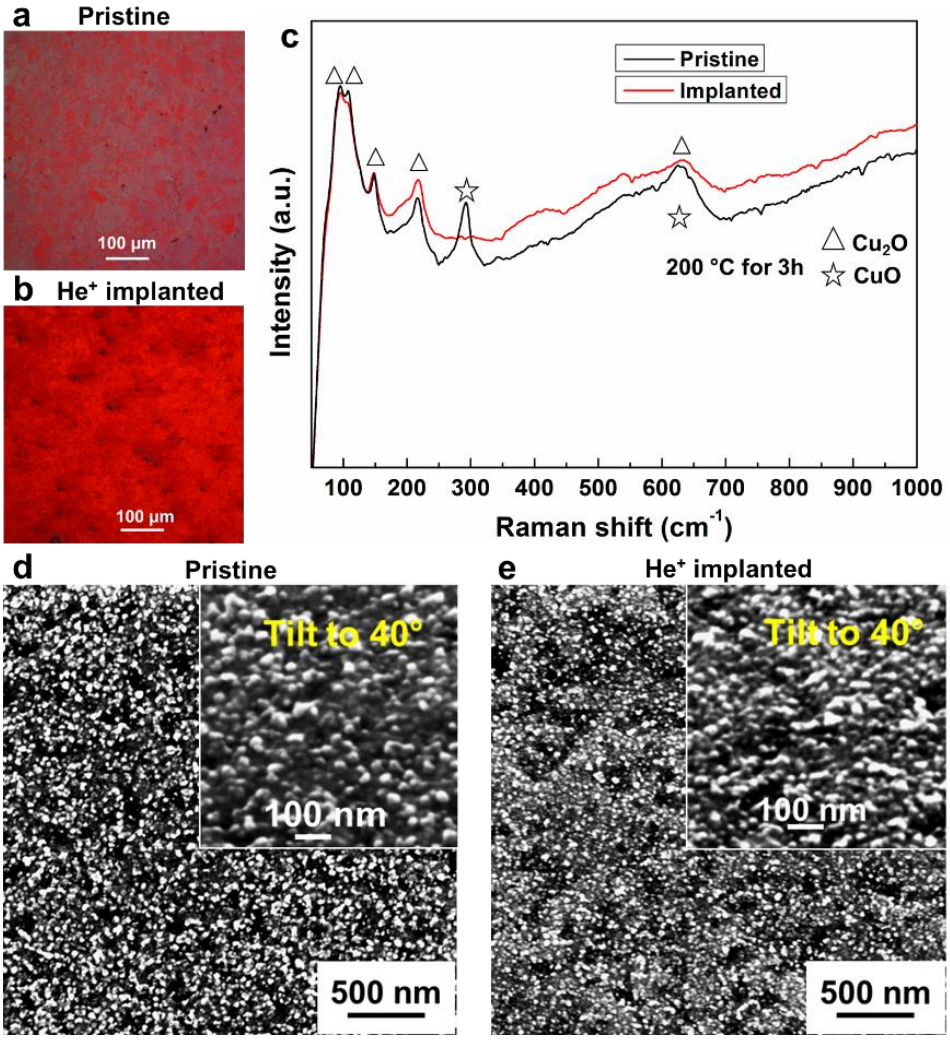

Fig. 4. (a, b) Optical images, (c) Raman spectra, and (d, e) SEM images of (a, d) pristine Cu and (b, e) He^+-implanted Cu after heating at 200 °C for 3 h. The insets to (c and d) were acquired at higher magnification with the sample tilted at 40°.

The SEM-EDS analyses showed that the carbon concentration on the sample surface was greatly increased after ion implantation (Table 1 and Fig. 5(a)). Notably, a very low concentration of C was also found on the pristine Cu, most likely as a result of contamination by the ambient environment. The large increase in the amount of C after He^+ implantation confirmed that

additional carbonaceous material was indeed introduced onto the Cu surface. This effect was attributed to contamination by the pump oil within the vacuum system [12]. Wide scan XPS data showed that only Cu, O and C were present on the sample surfaces (Fig. 5(b)). The spectrum obtained from the He^+-implanted Cu showed a lower Cu peak intensity along with a more intense C peak. These results suggest that a carbonaceous material covered the Cu surface after He^+ implantation. The injected He^+ ions, introduced by this implantation process, would not be expected to passivate Cu oxidation [8]. Furthermore, studies have reported that surface regions containing defects are more readily oxidized [2,25], suggesting that defects induced by He^+ implantation would also not be expected to inhibit Cu oxidation (and in fact might have the opposite effect by promoting oxidation) [8, 26]. Thus, the lower extent of Cu oxidation after He^+ implantation can be attributed to the carbonaceous material introduced onto the Cu surface.

Table 1. Surface compositions of various samples as determined by SEM-EDS.

Sample	C (at%)	Cu (at%)
Pristine	4.7 ± 1.4	95.3 ± 1.4
Implanted	30.5 ± 5.3	69.5 ± 5.3
Implanted + cleaned	7.8 ± 2.5	92.2 ± 2.5

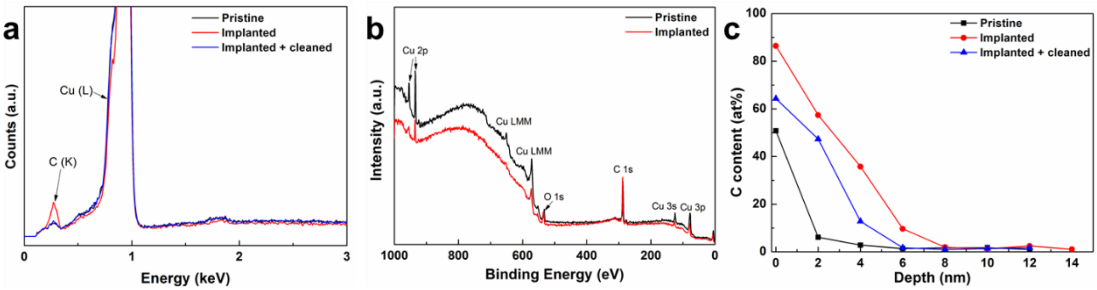

Fig. 5. (a) SEM-EDS spectra obtained from pristine Cu, He^+-implanted Cu and He^+-implanted Cu with subsequent surface cleaning. (b) XPS wide-scan spectra and (c) C depth profiles determined by XPS etching for some or all of the same samples.

It was found that the majority of the carbonaceous contamination could be removed simply by cleaning the He^+-implanted Cu using acetone and deionized water (Table 1 and Fig. 5(a)). However, even after thorough cleaning, this specimen exhibited a higher C content than that of the pristine material. Depth profiles acquired using XPS etching (Fig. 5(c)) demonstrated that C was implanted into the Cu along with the He^+ ions to a depth of approximately 4 nm. XPS spectra showing the O and Cu depth profiles are provided in Fig. S2. The He^+-implanted + cleaned Cu samples were also heated at 200 °C for different time spans and the surface colorations and morphologies of these materials indicated a passivation effect (Fig. 6) compared with the pristine Cu (Figs. 2–4). The surface color and morphology of each of these specimens were also very similar to those of the uncleaned He^+-implanted Cu. These results suggest the same inhibition of Cu oxidation, in keeping with the XPS etching results presented in Fig. 7. The C concentration depth profiles and the O/Cu concentration ratio depth profiles of samples after heating are displayed in Figs. 7(a) to 7(d). As a

result of the carbon contained in these materials, the O depth profiles may not clearly reflect the oxidation states of these three samples, as can be seen in Fig. S3. Consequently, the O/Cu concentration ratios are provided, with Cu_2O and CuO giving values of 0.5 and 1.0, respectively. As shown in Figs. 7(b) and 7(d), both the original and cleaned He^+-implanted Cu specimens exhibited lower oxide layer thicknesses compared with the pristine Cu, confirming that the carbonaceous contamination introduced on the surface inhibited oxidation. Moreover, it is apparent that the O/Cu concentration ratio depth profiles of the He^+-implanted Cu with and without subsequent surface cleaning were quite similar (Figs. 7(b) and 7(d)). Because most of the carbonaceous contamination absorbed on the surface was removed during cleaning Cu (Table 1 and Fig. 5(a)), this result confirms that the passivation effect of this contamination can be primarily attributed to C implanted below the surface of the material (Fig. 5(c)). It also seems that the oxidation inhibition effect required both the carbonaceous material and the ion implantation process, which decomposed the carbonaceous material and drove the resulting carbon into the Cu [27].

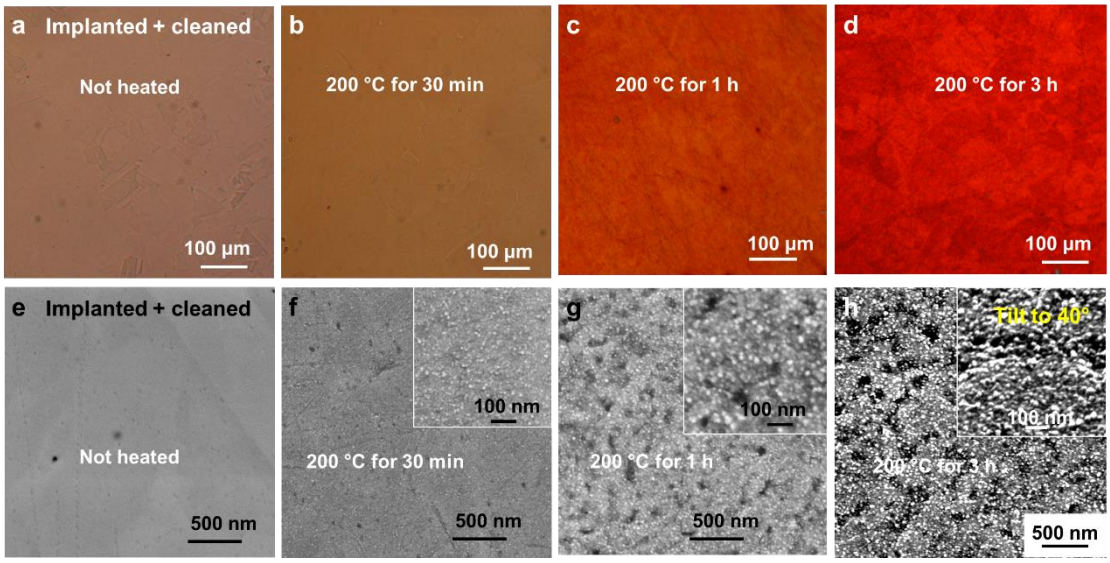

Fig. 6. (a-d) Optical and (e-h) SEM images of the surfaces of He^{+}-implanted + cleaned Cu specimens processed using different oxidation conditions.

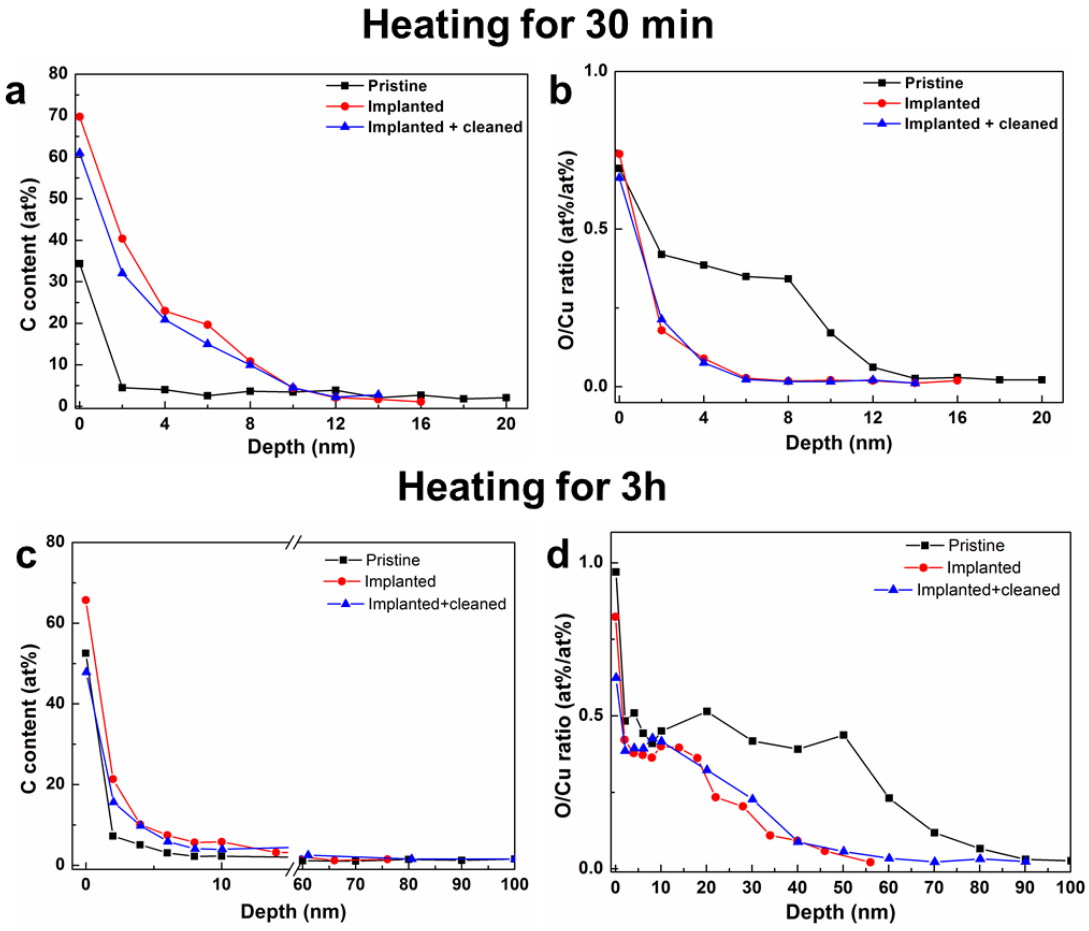

Fig. 7. (a, c) Carbon concentration depth profiles and (b, d) O/Cu concentration ratio

depth profiles of various samples as determined by XPS etching.

4. Discussion

It is obvious that the carbonaceous contamination introduced on the Cu surface during He^+ implantation protected the material from oxidation. However, the associated mechanism and microstructural evolution of these samples are unclear. Thus, TEM was used to examine the microstructures of the materials. Specifically, cross-sectional TEM and STEM images of pristine Cu after heating for 30 min are shown in Fig. 8. Studies have reported that the growth of Cu oxide on a clean Cu surface tends to proceed via the nucleation and coalescence of oxide islands [2,25]. Figure 8(a) shows that the pristine specimen had a rough surface with some island-like structures, which is consistent with previously reported results [2,28]. These island-like structures were found to comprise Cu_2O based on STEM-EDS analyses (inset to Fig. 8(b)) and HR-TEM observations (Fig. 8(c)) as well as the Raman (Fig. 2(c)) and XPS results (Fig. 7(a)). The fast Fourier transform (FFT) of the selected area shown in the right part of Fig. 8(c) shows that the Cu_2O islands grew epitaxially from the Cu substrate, in agreement with previously published data [2,29].

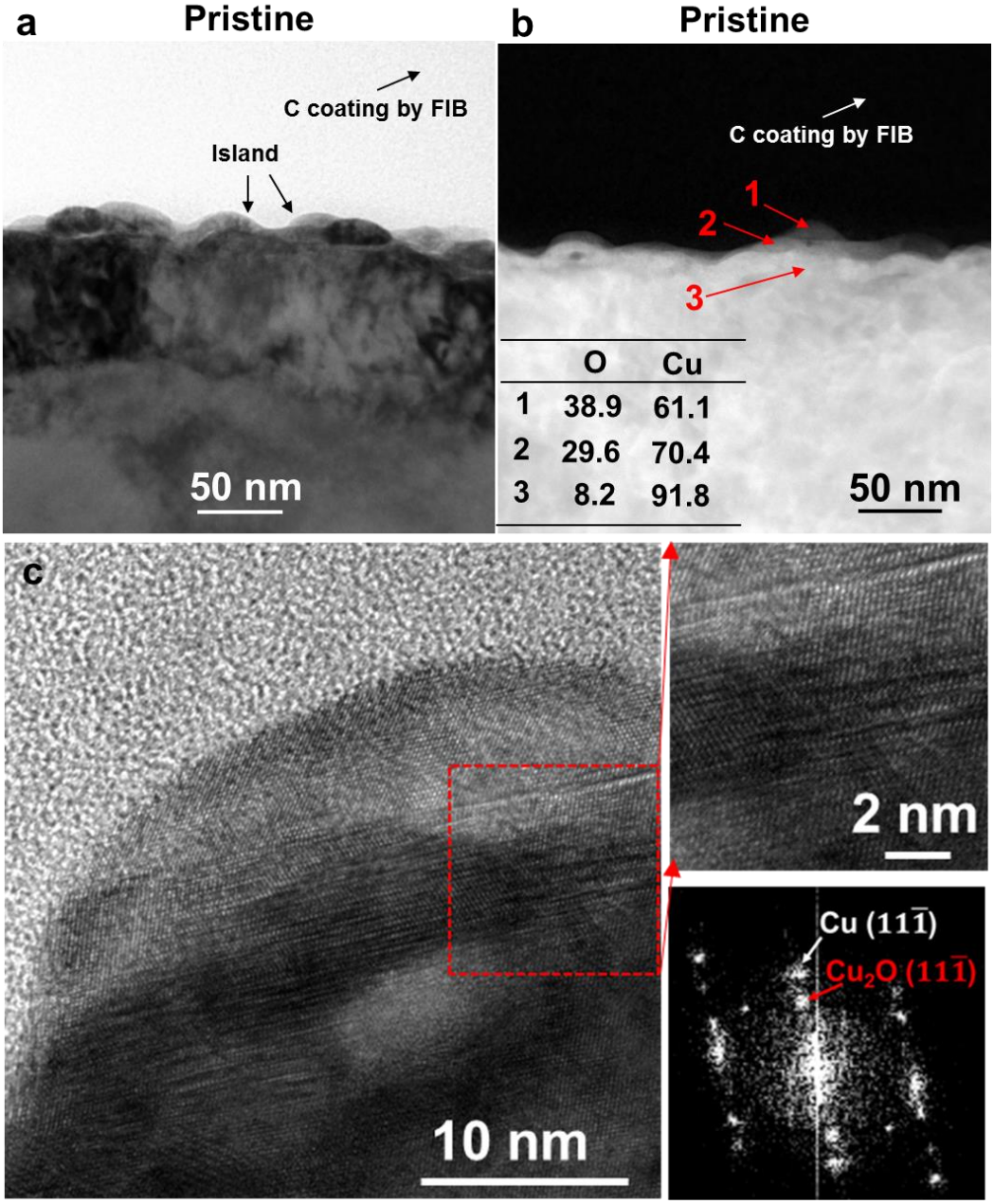

Fig. 8. (a) Bright-field cross-sectional TEM, (b) HAADF-STEM and (c) HR-TEM images of pristine Cu heated at 200 °C for 30 min. The two images in the right hand side of (c) are an enlarged view of a selected area and its FFT.

The surface of the He^+-implanted Cu after heating at 200 °C for 30 min was relatively smooth and did not show any obvious island-like structures

(Figs. 9(a) and 9(b). The bright-field TEM image (Fig. 9(a)) and HAADF-STEM image (Fig. 9(b)) of this material showed a relatively uniform and layer-like structure with a thickness of approximately 10 nm. This layer generated a brighter contrast than the Cu substrate in the bright-field TEM image and a weaker bright contrast in the HAADF-STEM image. HAADF-STEM analysis is sensitive to the atomic number of the sample, such that heavier elements usually produce a brighter contrast [30]. Thus, this layer structure was evidently composed of an element having a greater atomic number than that of carbon but lower than that of Cu. HR-TEM observations indicated that the layer structure exhibited minimal crystallinity and produced a relatively weak crystal lattice signal (Fig. 9(c)). The FFT of a selected area in this layer demonstrated the presence of Cu, Cu_2O and amorphous carbon. Notably, the C doped on the material during the FIB processing may have interfered with the FFT analysis for this amorphous C. However, when considering the XPS etching results shown in Fig. 7(a), it is clear that carbon was indeed present in this sample to a depth of approximately 10 nm from the surface. An HR-TEM image and inverse FFT image of this layer structure are also provided in Fig. S4, and confirm the combination of amorphous C, Cu and Cu_2O in this layer. Although a Cu_2O FFT phase can be observed in the FFT patterns (Figs. 9(c) and S4(a)), its intensity is always very weak, indicating that the Cu_2O concentration in this layer was relatively low. This result is in keeping with the XPS etching data in Fig. 7(b), in which the O/Cu concentration ratio in the He^+-implanted Cu was much lower than the value of 0.5 (equivalent to Cu_2O) in the surface

region (10 nm in depth). Thus, this layer consisted of C, Cu and a small amount of Cu_2O. This region is referred to as the C+Cu+Cu_2O layer herein for the sake of simplicity.

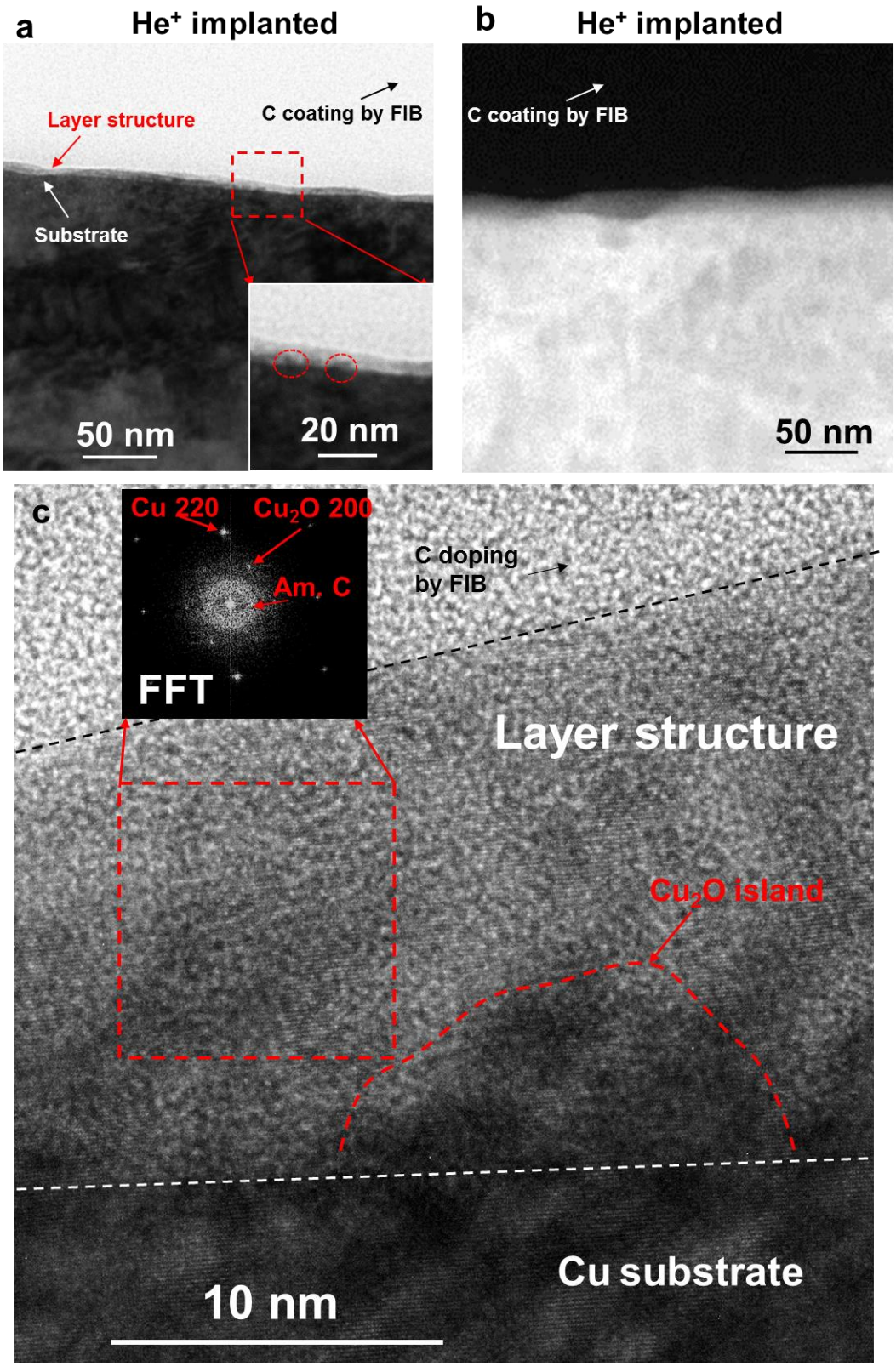
a
He+ implanted
Layer structure
C coating by FIB
Substrate
50 nm
20 nm
b
He+ implanted
C coating by FIB
50 nm
c
Cu 220
Cu2O 200
Am. C
FFT
C doping
by FIB
Layer structure
Cu2O island
Cu substrate
10 nm

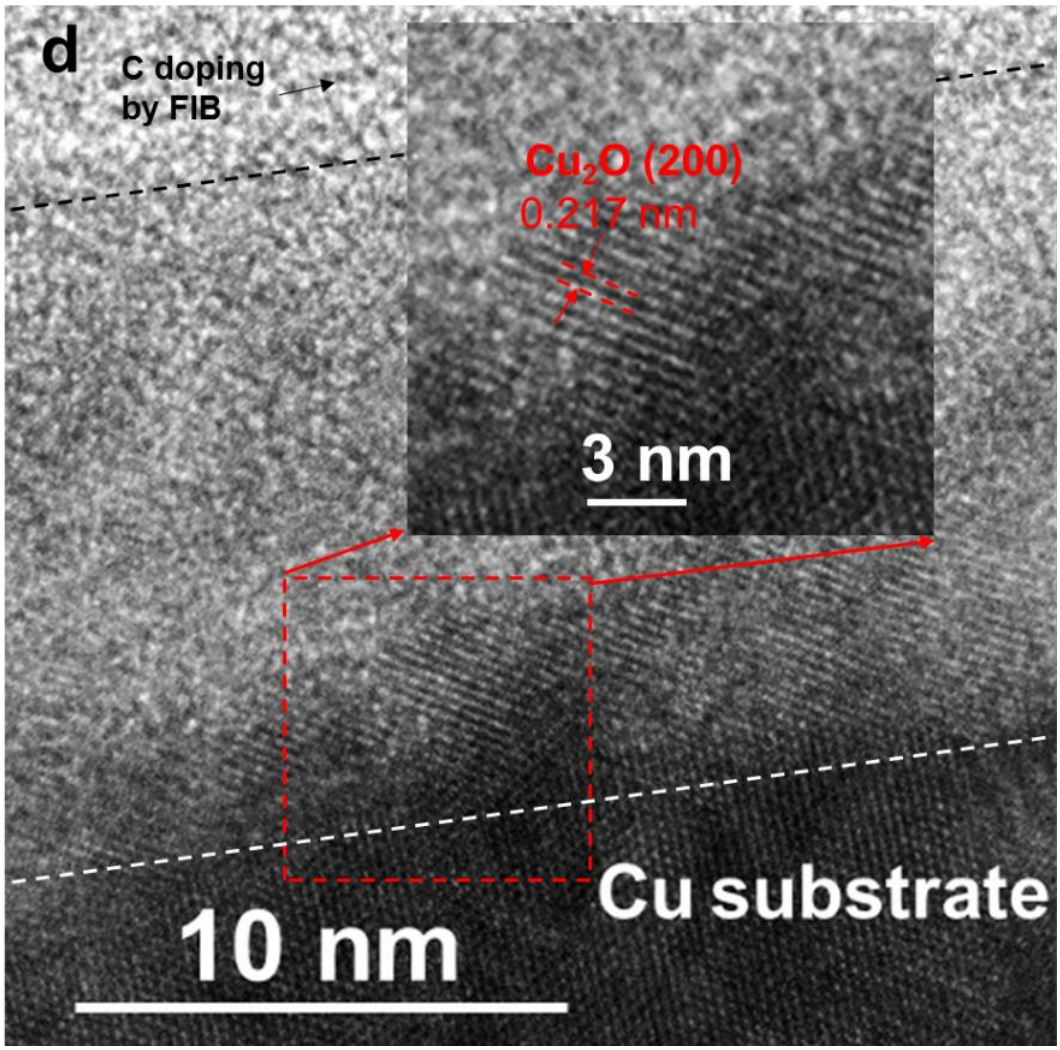

Fig. 9. (a) Bright-field cross-sectional TEM, (b) HAADF-STEM and (c) HR-TEM images of the surface of He^+-implanted Cu heated at 200 °C for 30 min. The inset is an FFT of the selected area. (d) Small Cu_2O islands formed on the He^+-implanted Cu after heating at 200 °C for 30 min. The inset is an enlarged view of the selected area.

This layer structure also appeared in the He^+-implanted + cleaned Cu prior to heating, as shown in the Fig. 10(a). This result was in keeping with the XPS spectra in Figs. 5(c) and S2(f), meaning that C was implanted below the surface of the Cu along with the formation of a small amount of Cu_2O (Fig.

1(e)). The formation of this C+Cu+Cu_2O layer is attributed to the C implanted into the Cu surface (Fig. 5(c)). A slight increase in the thickness of this layer structure was observed after heating for 30 min, as shown in Fig. 10(b). According to the XPS etching results in Figs. 7(a) and 5(c), the depth to which C was distributed increased from approximately 4 nm (Fig. 5(c)) to 10 nm (Fig. 7(a)) after heating the sample at 200 °C for 30 min. This result provided further evidence that the formation of this layer was a consequence of the C introduced into the Cu. The increased thickness of this layer after heating may be attributed to the interdiffusion of the C and Cu during heating, as well as to the formation of Cu and C oxides.

Figure 9(a) demonstrates the formation of some small Cu_2O islands at the interface between the Cu substrate and the C+Cu+Cu_2O layer, corresponding to the HR-TEM image in Fig. 9(d). Because these islands were below the C+Cu+Cu_2O layer, they appear to have formed based on the absorption of oxygen diffusing through the C+Cu+Cu_2O layer. It is interesting to note that, although some Cu was present in this C+Cu+Cu_2O layer (Figs. S3(b) and 9(c)) and some oxygen diffused through this layer, the Cu in this layer was not heavily oxidized (Fig. 7(b)). In fact, Cu_2O was preferentially formed on the Cu substrate, indicating that the oxidation of Cu in this layer was suppressed as a consequence of the presence of carbon in this layer. Because the Cu_2O islands were formed on the Cu substrate by absorbing the oxygen diffusing through the C+Cu+Cu_2O layer and C compounds (such as graphene) improve Cu oxidation resistance by acting as a barrier to gas diffusion [19,20], the formation of this layer may have protected the Cu substrate from

oxidation by hindering oxygen ingress.

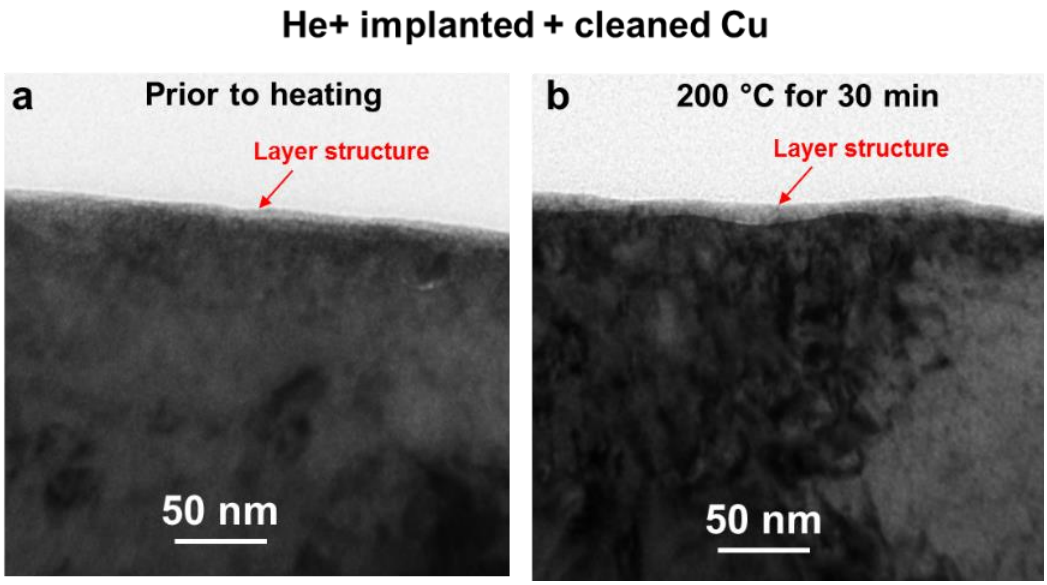

Fig. 10. Microstructure of a He^{+}-implanted Cu sample with subsequent surface cleaning (a) before heating and (b) after heating at 200 °C for 30 min.

TEM images of a Cu specimen heated for 3 h are provided in Fig. 11. It is evident that an oxide layer was formed on the pristine Cu by the coalescence of oxide islands to a thickness of approximately 58 ± 19 nm, in keeping with the XPS etching results (Fig. 7(d)). Several void-like structures also appeared on the Cu substate as a result of the Kirkendall effect [31]. In the case of the He^{+}-implanted Cu, the degree of oxidation varied over the surface, and three representative areas are shown in Figs. 11(b) to 11(d). In Fig. 11(b), a thin C+Cu+Cu_2O layer is apparent on the Cu surface with some small Cu_2O islands at the interface between the Cu substrate and the C+Cu+Cu_2O layer, similar to the appearance of the sample in Fig. 9(a). Several larger islands can also be seen in Fig. 11(c) under the C+Cu+Cu_2O layer, indicating that

the formation of these islands should be ascribed to the growth and coalescence of smaller islands based on the continued absorption of oxygen diffusing through the C+Cu+Cu_2O layer. The Cu_2O islands preferentially formed and grew on the C+Cu+Cu_2O/Cu interface rather than the air/C+Cu+Cu_2O interface, suggesting that the oxidation rate in this sample was determined by the rate of oxygen diffusion from the ambient air to the Cu substrate. Comparing the oxide layer thickness in the Fig. 11 (b) with 9(a) (He^+-implanted Cu) and Fig. 11(a) with 8(a) (pristine Cu), as well as the XPS-etching results in Fig. 7(d) with 7(b), these analyses demonstrate that the rate of growth of the oxide layer on the He^+-implanted Cu was lower than that on the pristine Cu as the heating time was increased from 30 min to 3 h. Because the formation and growth of Cu_2O on the He^+-implanted Cu proceeded in conjunction with the diffusion of oxygen through the C+Cu+Cu_2O layer, the lower oxide growth rate on this sample indicates that this C+Cu+Cu_2O layer created a barrier to the diffusion of oxygen. In fact, studies have reported that oxygen can readily diffuse into a Cu substrate through grain boundaries and dislocations [8,32]. As shown in Figs. 8(a) and 11(a), the oxide layer on the pristine Cu was generated as a consequence of the coalescence of oxide islands, and so this layer would be expected to contain numerous grain boundaries providing paths for oxygen diffusion. However, a C+Cu+Cu_2O layer may block these paths, resulting in a decreased oxidation rate. Figure 11(d) indicates the loss of this C+Cu+Cu_2O layer on the He^+-implanted Cu sample that showed a higher degree of oxidation as compared with the specimens in Figs. 11(b) and 11(c). This area

exhibits a thicker oxidation layer and the appearance of void-like structures, resulting from the Kirkendall effect. These data provide additional evidence that the C+Cu+Cu_2O layer formed on the He^+-implanted Cu protected the metal from oxidation by providing a barrier to the diffusion of oxygen. Therefore, it is clear that the inhibited Cu oxidation effect of the carbonaceous contamination was realized by the formation of a special C+Cu+Cu_2O layer on the surface of the Cu substate that blocked the ingress of oxygen.

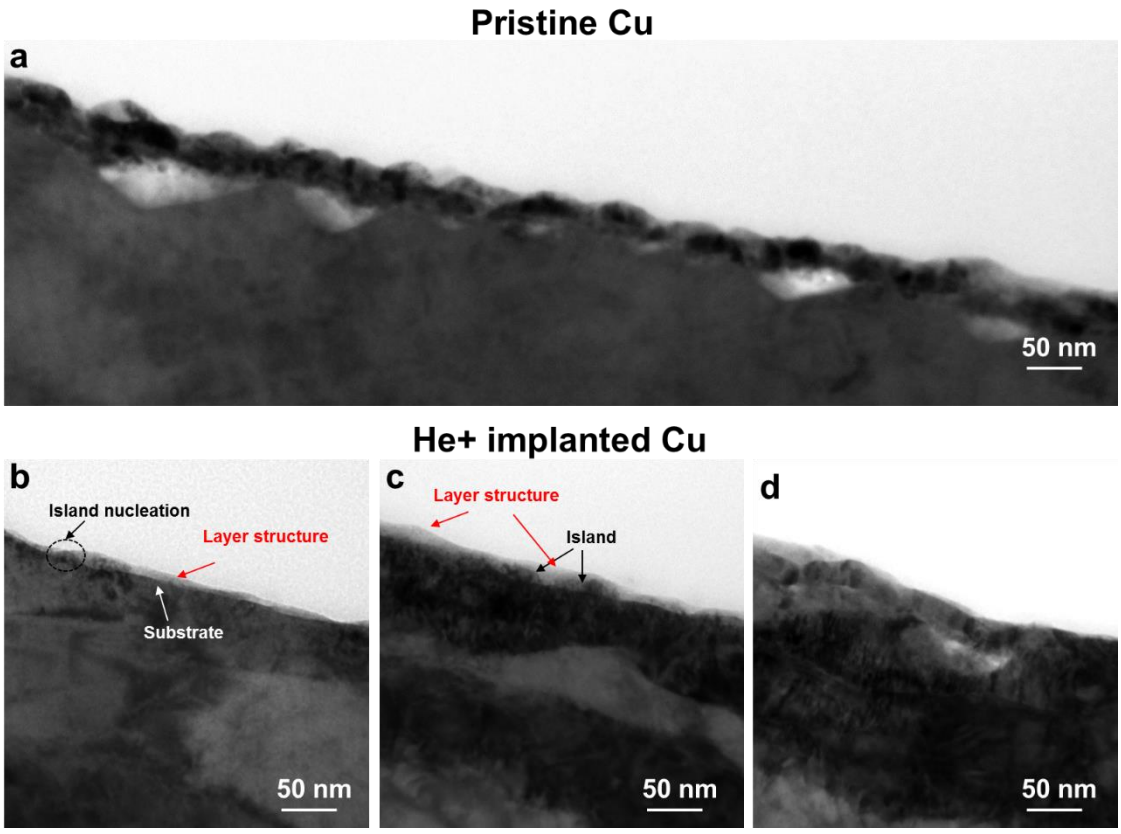

Fig. 11. TEM images of (a) pristine Cu and (b-d) different areas of He^+-implanted Cu after heating for 200 °C for 3 h.

With regard to the disappearance of this C+Cu+Cu_2O layer, the present

assessments show that the ongoing growth of Cu_2O islands on the He^+-implanted Cu caused these islands to break through the layer after reaching a critical size (Fig. 12(a)). At the areas where the Cu_2O was in direct contact with ambient air (that is, the regions at which the oxide burst through), the Cu_2O exhibited more rapid growth than the other areas that were still covered by the C+Cu+Cu_2O layer (Fig. 12(b)). This result suggests faster oxygen diffusion at the former regions. Figure 12(b) demonstrates that the thickness of this C+Cu+Cu_2O layer gradually decreased in the vicinity of these breakthrough areas. Because this layer structure also contained Cu, more rapid oxygen diffusion at the bursting areas may also have increased the oxidation of Cu in the C+Cu+Cu_2O layer, leading to faster removal of this layer. As discussed above, the passivation effect of this layer was ascribed to the presence of C. However, the C content in this layer was decreased as oxidation progressed (Figs. 7(a) and 7(c)). This phenomenon may be attributed to the diffusion of C into the Cu substrate or to the consumption of C during oxidation. As a result, the oxidation inhibition effect of this layer was decreased, and the layer disappeared more rapidly.

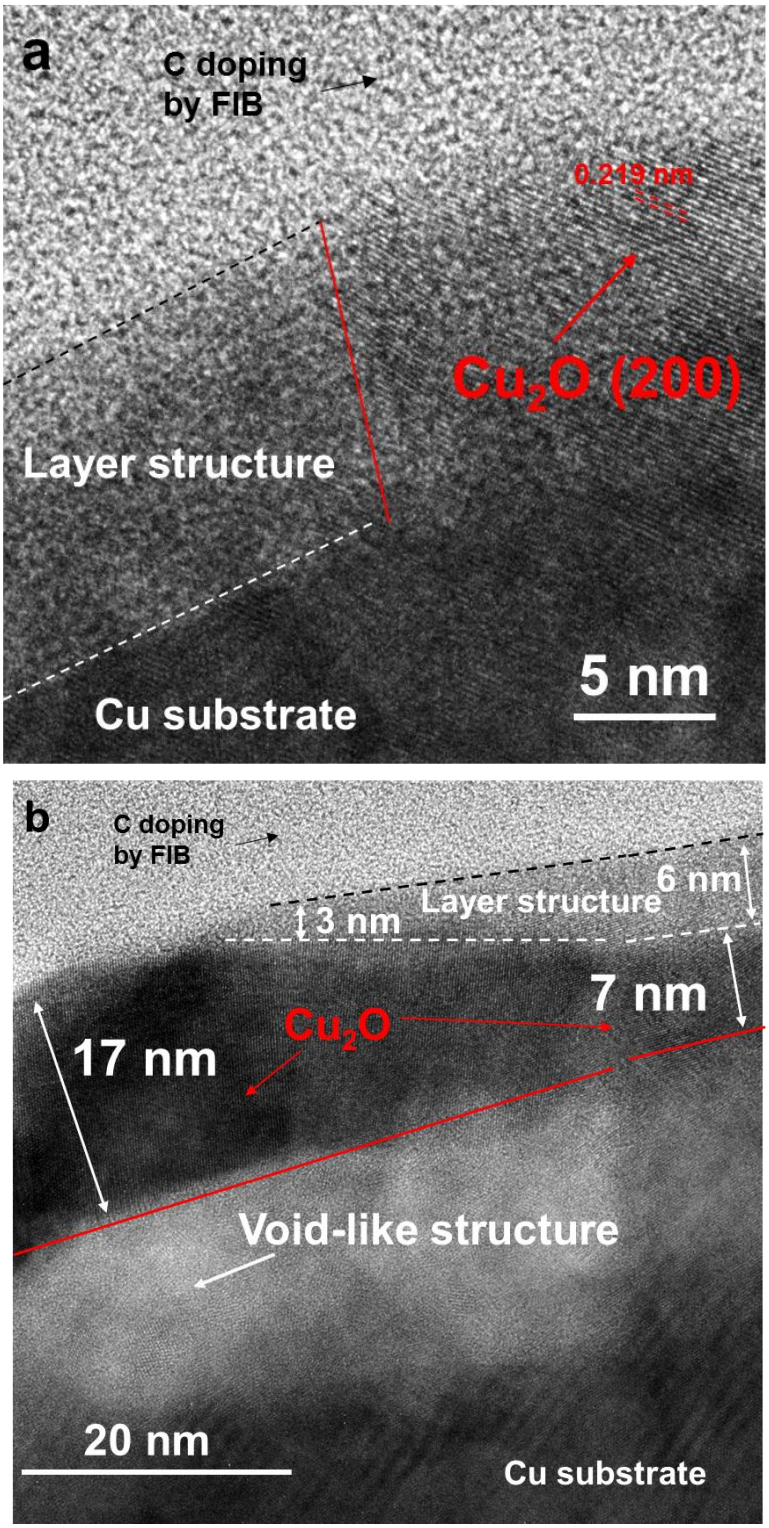

Fig. 12. HR-TEM images of a He^{+}-implanted Cu sample after heating at 200 °C for 3h. (a) The area in which Cu_2O islands broke through the C+Cu+Cu_2O layer. (b) The area in which the C+Cu+Cu_2O layer disappeared.

5. Conclusion

The oxidation of Cu with and without He^+ implantation was investigated. The data show that carbonaceous contamination was definitely deposited on the Cu surface during this process and subsequently inhibited oxidation of the Cu as a consequence of C implanted below the surface. This passivation effect resulted from the formation of a special layer structure made of C and Cu along with a small amount of Cu_2O that served as an oxygen diffusion barrier. This information should be helpful in the future application of ion implantation as a means of preventing Cu oxidation, and also provides a better understanding of the effects of carbonaceous materials on the Cu oxidation process.

Acknowledgement

This work was supported by JSPS KAKENHI grant numbers JP19K22035 and JP19H00799. Part of this work was conducted at the Joint-Use Facilities at Hokkaido University, supported by the Project for Promoting Public Utilization of Advanced Research Infrastructure (Program for Supporting Introduction of the New Sharing System) under grant number JPMXS0420100519 and by the Nanotechnology Platform program of the Ministry of Education, Culture, Sports, Science and Technology (MEXT), Japan. The authors thank Mr. R. Ota for his help with the STEM analyses. Dr. Yang acknowledges stipend support from the Chinese Scholarship Council to perform this work at Hokkaido University. We thank Edanz (https://jp.edanz.com/ac) for editing a draft of this manuscript.

References

[1] J. Peng, B. Chen, Z. Wang, J. Guo, B. Wu, S. Hao, Q. Zhang, L. Gu, Q. Zhou, Z. Liu, S. Hong, S. You, A. Fu, Z. Shi, H. Xie, D. Cao, C. Lin, G. Fu, L. Zheng, Y. Jiang, N. Zheng, Surface coordination layer passivates oxidation of copper, Nature, 586 (2020) 390-394.

[2] A. M. Chiara Gattinoni, Atomistic details of oxide surfaces and surface oxidation: the example of copper and its oxides, Surf. Sci. Rep. 70 (2015) 424–447.

[3] J. Liu, H. Jiang, L. Zhang, H. Gu, X. Chen, S. Liu, Thickness dependent native oxidation kinetics observation and prediction for Cu films using spectroscopic ellipsometry, Appl. Surf. Sci. 518 (2020) 146236.

[4] Y. Xu, Y. Chen, P. Schützendübe, S. Zhu, Y. Huang, Z. Ma, Y. Liu, Z. Wang, Thermal oxidation of amorphous Cu_xZr_{1-x} alloys: Role of composition-dependent thermodynamic stability, Appl. Surf. Sci. 503 (2020) 144376.

[5] J. Song, L. Wang, A. Zibart, C. Koch, Corrosion Protection of Electrically Conductive Surfaces, Metals 2 (2012) 450–477.

[6] Y. Qiang, S. Zhang, H. Zhao, B. Tan, L. Wang, Enhanced anticorrosion performance of copper by novel N-doped carbon dots, Corros. Sci. 161 (2019) 108193.

[7] Y. Qiang, S. Zhang, L. Guo, X. Zheng, B. Xiang, S. Chen, Experimental and theoretical studies of four allyl imidazolium-based ionic liquids as green inhibitors for copper corrosion in sulfuric acid, Corros. Sci. 119 (2017) 68–78.

[8] C. J. McHargue, Ion implantation in metals and ceramics, International Metals Reviews, 31 (1986) 49.

[9] Y. Zhang, W. J. Weber, Ion irradiation and modification: The role of coupled electronic

and nuclear energy dissipation and subsequent nonequilibrium processes in materials, Appl. Phys. Rev. 7 (2020) 41307.

[10] Z. Qin, Q. Luo, Q. Zhang, Z. Wu, L. Liu, B. Shen, W. Hu, Improving corrosion resistance of nickel-aluminum bronzes by surface modification with chromium ion implantation, Surf. Coat. Technol. 334 (2018) 402–409.

[11] X. Q. Zhao, Modification of oxidation resistance of copper films by shallow implantation, J. Appl. phys. 90 (2001) 1638–1641.

[12] M. Y. Tsai, B. G. Streetman, R. J. Blattner, C. A. Evans, Jr., Study of Surface Contamination Produced during High Dose Ion Implantation, J. Electrochem. Soc. 126 (1979) 98–102.

[13] A. J. Kellock, M. H. Tabacniks, J. E. E. Baglin, N. S. Somcio, T. T. Bardin, D. C. Miller, Mechanism for ion beam passivation of copper surfaces, Nucl. Instrum. Methods Phys. Res. B 127/128 (1997) 742–746.

[14] W. Jin, G. Wu, H. Feng, W. Wang, X. Zhang, P. K. Chu, Improvement of corrosion resistance and biocompatibility of rare-earth WE43 magnesium alloy by neodymium self-ion implantation 94 (2015) 142–155.

[15] X.B. Tian, C. B. Wei, S. Q. Yang, R. K. Y. Fu, P. K. Chu, Corrosion resistance improvement of magnesium alloy using nitrogen plasma ion implantation, Surf. Coat. Technol. 198 (2005) 454–458.

[16] R. I. M. Asri, W. S. W. Harun, M. Samykano, N. A. C. Lah, S. A. C. Ghani, F. Tarlochan, M. R. Raza, Corrosion and surface modification on biocompatible metals: A review, Mater. Sci. Eng. C 77 (2017) 1261–1274.

[17] T. R. Rautray, R. Narayanan, K. H. Kim, Ion implantation of titanium based biomaterials, Progr. Mater. Sci 56 (2011) 1137–1177.

[18] P. Vlcak, J. Fojt, Z. Weiss, J. Kopeček, V. Perina, The effect of nitrogen saturation on the corrosion behaviour of Ti-35Nb-7Zr-5Ta beta titanium alloy nitrided by ion implantation, Surf. Coat. Technol. 358 (2019) 144–152.

[19] D. W. Kang, J. Y. Kwon, H. Cho, J. H. Sim, H. S. Hwang, C. S. Kim, Y. J. Kim, R. S. Ruoff, H. S. Shin, Oxidation Resistance of Iron and Copper Foils Coated with Reduced Graphene Oxide Multilayers, ACS Nano 6 (2012) 7763–7769.

[20] M. Ans, Monolayered graphene oxide as a barrier on polycrystalline copper substrate against thermal oxidation for a long duration, J. Electroanalytical Chem. 895 (2021) 115526.

[21] J. F. Ziegler, M. D. Ziegler, J. P. Biersack, SRIM – The stopping and range of ions in matter (2010), Nucl. Instrum. Methods Phys. Res. B 268 (2010) 1818–1823.

[22] W. J. Weber, Y. Zhang, Predicting damage production in monoatomic and multi-elemental targets using stopping and range of ions in matter code: Challenges and recommendations, Curr. Opin. Solid state Mater. Sci. 23 (2019) 100757.

[23] D. Powell, A. Compaan, J. R. Macdonald, Raman-scattering study of ion-implantation-produced damage in Cu_2O, Phys. Rev. B 12 (1975) 20–25.

[24] N. Bodappa, M. Su, Y. Zhao, J. Le, W. Yang, P. Radjenovic, J. Dong, J. Cheng, Z. Tian, J. Li, Early stages of electrochemical oxidation of Cu(111) and polycrystalline Cu surfaces revealed by in situ Raman spectroscopy, J. Am. Chem. Soc. 141 (2019) 12192−12196.

[25] G. Zhou, L. Wang, J. C. Yang, Effects of surface topology on the formation of oxide islands on Cu surfaces, J. Appl. phys. 97 (2005) 63509.

[26] N. Daghbouj, B. S. Li, M. Callisti, H. S. Sen, J. Lin, X. Ou, M. Karlik, T. Polcar, The structural evolution of light-ion implanted 6H-SiC single crystal: Comparison of the

effect of helium and hydrogen, Acta Mater. 188 (2020) 609-622.

[27] E. H. Hirsch, The growth of carbonaceous contamination on surfaces undergoing ion bombardment, J. Phys. D: Appl. Phys. 10 (1977) 2069–2076.

[28] G. Zhou, J. C. Yang, Temperature effects on the growth of oxide islands on Cu(1 10), Appl. Surf. Sci. 222 (2004) 357–364.

[29] G. Zhou, L. Luo, L. Li, J. Ciston, E. A. Stach, W. A. Saidi, J. C. Yang, In situ atomic-scale visualization of oxide islanding during oxidation of Cu surfaces, Chem. Commun. 49 (2013) 10862–10864.

[30] S. Yang, Y. Nakagawa, M. Kondo, T. Shibayama, Anisotropic defect distribution in He + -irradiated 4H-SiC: Effect of stress on defect distribution, Acta mater. 221 (2021) 116845.

[31] A. Paul, M. J. H. van Dal, A. A. Kodentsov, F. J. J. van Loo, The Kirkendall effect in multiphase diffusion, Acta mater. 52 (2004) 623–630.

[32] S. Lee, H. Hsu, W. Tuan, Oxidation Behavior of Copper at a Temperature below 300 °C and the Methodology for Passivation, Mater. Res. 19 (2016) 51–56.